Figure Captions

Figure 1. Photo of the meteotsunami wave impacting the shore at Zandvoort, North Holland. This is taken from a video by Jan Koning (https://www.youtube.com/watch?v=CjQk_xt_WU01).

Figure 2. Synoptic analysis 0000UTC 29 May 2017. The upper cold front (white triangles) has run ahead of the surface cold front (black triangles) near Low LA 1012 near Brittany, with High HA1021 over Europe.

Figure 3. Locations of observational reports mentioned in the text, including of tide gauge data in Table 1. The Red line from Dover to Calais shows the location of the cross section used in the 2D model. Point S is the location of the Sandettie Light Vessel, and point E is the Europlatform. The inset box shows the north coast of the Netherlands and Germany. The bathymetry map is courtesy of the NOAA NCEI.

Figure 4. Mean sea level pressure (MSLP) readings (hPa) at Herstmonceux (East Sussex), Langdon Bay (Kent) and Manston (Kent). Time is in UTC. The pressure spike becomes higher and more pronounced further east.

Figure 5. Simplified cross-section of gravity wave running beneath elevated convection, running from WSW towards the ENE. The boundary layer airflow is from the ENE to WSW, shown in green. The rear flank downdraft in red, and storm relative inflow in blue. The downdraft evidently penetrated to the surface as indicated by the Sandettie Light Vessel observation. The low-level gravity wave is shown as a dotted black line running with the storm system. This image is adapted from Marsham et al. (2010).

Figure 6a. Selected tide gauge data with sites between Jersey in the English Channel, to Hornum on the coast of Germany. These show residual water levels (total water level minus the astronomical tide). Jersey and the English gauges (Dover, Harwich, Lowestoft) are at 15-minute cadence, while the French and German gauges are at 1-minute cadence. Data has been downloaded from the EC JRC database. ttps://webcritech.jrc.ec.europa.eu/SeaLevelsDb/Home

Figure 6b. Tide gauge graphs (in cm) from the Netherlands, Rijkswaterstaat – sourced from Sluijter, et al. (2017), and Helzel Messtechnik, (2017). The Europlatform graph (top-left) is 1-minute data (green), 10-minute moving averages (blue), and residual water level (purple). The other graphs, Ijmuiden, Scheneningen and Oosterschelde, show the residual water level in (light blue), the total water level (purple), and the astronomical tide (green). These are at 10-minute cadence. Time is UTC plus 2 hours.

Figure 7. Rain radar images from the UK composite network covering southern Britain, the English Channel, North France, Belgium and southern tip of the Nertherlands. The bow-shaped echoes can be most clearly seen between 0100-0300UTC running from Southeast England to The Netherlands.

Figure 8. Trappes (Paris) radiosonde vertical profile of the atmosphere. The grey automated construction represents the idealised elevated convective storm updraft to the tropopause, with CAPE of 619 Jkg-1. The shaded grey area bounded by thr blue construction represents idealised

DCAPE from around 600 hPa to surface. The red area indicates the relevant layer of warm advection. Plotted online at University of Wyoming: (http://weather.uwyo.edu/upperair/europe.html).

Figure 9. MSG InfraRed satellite image sequence 29/0200 UTC to 0500 UTC. Cold, dense, high level cloud is whiter. A darkening band can be seen developing in the rear of the storm (shown by the yellow arrow at 0400UTC), possible indicative of the presence of downdraft as air is warmed with cloud decreasing. MSG cloud top heights (top left), which is supported by atmospheric observations of temperature pressure on the Trappes ascent. Plotted by the Met Office. © Crown Copyright.

Figure 10. Ijmuiden radiosonde vertical profile of the atmosphere 29/0300 UTC. This most clearly shows the ENE flow in the boundary layer (below ~900 hPa) with a temperature inversion ahead of the storm. There is marked change in direction and speed above the boundary layer. (source: KNMI, Creative Commons zero (CC0) statement.

Figure 11. Cabauw UV LIDAR showing the low-level gravity wave in the boundary layer with a sudden jump in height between 0400 and 0500 UTC. The white colour indicates cloud, while the green, yellow and brown is indicative of particulate matter that provides a marker for atmospheric changes (source: KNMI, Creative Commons zero (CC0) statement).

Figure 12. Herstmonceux radiosonde ascent failed above 650 hPa. But it shows broadly easterly winds below 900 hPa, followed by a marked veer to a southwesterly direction. The main cloud base appears around 800 hPa (~2000 m). Plotted online at University of Wyoming: (http://weather.uwyo.edu/upperair/europe.html).

Figure 13. Figure 13. Met Office UKV NWP high resolution operational forecast (left), and the equivalent parallel suite model run (PS39) (right). Both show cloud, precipitation and surface pressure isobars. It is notable that there are marked differences in the shape of the MCS, and no evidence of a meso-high. DT: 28/1800UTC / VT: 29/0300UTC (T+9 hour forecast from 28/1800UTC). © Crown Copyright.

Figure 14. Illustrative 2D model and table of a cross-section from Dover to Calsais at approximately 1.12 km resolution. This simply calculates the Froude number at different wind speeds between 14 and 28 ms^{-1} to determine where Proudman resonance is likely (shaded red). Given a wind speed of 18 to 20 ms^{-1} , it can be seen that at 18 ms-1, resonance is most effective on the Dover side, and at higher speeds on the Calais side. The course bathymetry in the cross section is plotted below.

Convective rear-flank downdraft as driver for meteotsunami along English Channel and North Sea coasts 28-29 May 2017

Andrew M. Sibley 1, Dave Cox 2, and David R. Tappin 3 & 4

1 Met Office, Hazard Centre, Fitzroy Road, Exeter, UK, EX12 3PB
2 Met Office, Flood Forecasting Centre, Fitzroy Road, Exeter, UK, EX12 3PB
3 British Geological Survey, Keyworth, Nottingham, NG12 5GG
4 Department of Earth Sciences, University College London (UCL), London

Abstract

We examine the physical processes that led to the meteotsunami observed along the English Channel and North Sea coasts on 29 May 2017. It was most notably reported along the Dutch coast, but also observed on tide gauges from the Channel Islands to the coast of Germany, and also those in eastern England. From an assessment of multiple observations, including rain radar, LIDAR, satellite, surface observations and radiosonde reports we conclude that the event was driven by a rear flank downdraft in association with a mesoscale convective system (MCS). This downdraft, from a medium level or elevated MCS, led to a hydrostatically forced internal or ducted gravity wave below the MCS. The gravity wave was manifested by a marked rise and fall in pressure, a meso-high, which then interacted with the sea surface through Proudman resonance causing a measured wave of close to 0.9 m in amplitude, and an estimated wave run-up on Dutch beaches of 2m. Through examination of existing research we show that the basic assumptions here relating to the formation of the Dutch meteotsunami, are consistent with previously described physical processes, and confirms the correlation between the speed of the ocean wave and medium level steering winds. This raises the possibility that high-resolution, coupled, weather-ocean numerical weather prediction (NWP) models can be utilised to predict future events. However, deterministic high resolution NWP models still struggle with modelling convective systems with sufficient precision because of the chaotic nature of the atmosphere and incomplete observations. A way forward is proposed here to improve forecasting through post-processing of NWP model output by over laying medium level wind fields with ocean bathymetry.

Introduction

In the early morning of the 29 May 2017, a meteotsunami wave, estimated at 2 m in amplitude from some reports struck the coast of the Netherlands, resulting in damage to boats and a number of shoreline facilities (Sluijter et al. 2017; Assink et al. 2018). The estimation of 2 m is considered to be related to the breaking coastal wave or beach run-up. In terms of the observed amplitude, the wave was recorded on tide gauges in northern France, southeast England and Germany, with an amplitude of up to 0.88 m (Helzel, 2017). It was also spectacularly recorded on several video clips, for example at Zandvoort, and Katwijk aan Zee, which provided valuable evidence on the event. This is one of the first times a wave of this type and scale has been recorded on video (https://www.youtube.com/watch?v=CjQk_xt_WU01 accessed 09/01/2020) (Figure 1). The beaches inundated by the wave were popular tourist destinations, but fortunately, the meteotsunami struck before these were crowded, otherwise the human casualties would have been larger.

A meteotsunami is an ocean, or lake, wave with tsunami-like characteristics, but generated by meteorological conditions, such as rapid changes in air pressure. Through resonant interactions

between the atmospheric forcing and the water surface, the wave may grow until it becomes a risk to people present near impacted coasts. Further wave enhancement may occur in harbours, bays and estuaries, with seicheing continuing for a few hours in closed water bodies. The tsunami wave period is typically of the order of a few minutes to several hours, although wave amplitudes are smaller than the largest tsunamis generated by geological mechanisms, such as earthquakes and landslides (Monserrat et al, 2006; Rabinovich, 2020). Analysis of the synoptic patterns, and observational instrumentation that led to the formation of the meteotsunami wave, reveals the atmospheric characteristics. The synoptic analysis for this event is shown in Figure 2, and places mentioned in the text on the map of Figure 3.

In this paper, we show that the English Channel and North Sea meteotsunami was generated by an elevated Mesoscale Convective System (MCS), together with an associated atmospheric internal or ducted gravity wave (so-called because gravity is the restoring force to equilibrium following displacement in a fluid) running with the storm system at low levels. This low-level gravity wave is revealed by high-resolution pressure readings from southeast England, which show a marked surface pressure anomaly running with the storm system, referred to as a meso-high. At Langdon Bay, for example, there was a pressure rise of 4 or 5 hPa over periods as short as ten minutes, followed by a fall of similar magnitude (Figure 4). Pressure changes of 5 hPa were also recorded in the Netherlands, at De Kooy, Vlissingen, and Hoek van Holland (Port of Rotterdam) (Sluijter et al. 2017, Assink et al. 2018). Similar low-level gravity waves, and marked pressure changes have been described in meteotsunami events in the Adriatic (Šepić et al. 2009), and at Daytona Beach in Florida USA (Churchill et al. 1995). A representative diagram adapted from Marsham et al. (2010), and similar to textbook diagrams (Houze et al. 1989; Markowski and Richardson, 2010) of a storm associated with a meteotsunami, is shown in Figure 5, which is modified to illustrate an elevated convective system.

Air pressure measurements recorded with this meteotsunami suggest that it was forced and enhanced by an atmospheric gravity wave, with an associated meso-high acting upon the sea surface. The inverse barometer effect is small, of the order of 1 cm sea depression per 1 hPa pressure rise, but resonant enhancement of the wave was through Proudman resonance (Proudman, 1929). The resonance results from the atmospheric gravity wave, with an associated surface pressure change, that travels, approximately, at the same speed and direction as the sea surface wave (Tappin et al. 2013; Pattiaratchi and Wijeratne, 2015; Williams et al. 2019). Further enhancement of the wave, as it approaches the shoreline, may take place through Greenspan resonance, with an along-shore pressure disturbance acting upon shoreline edge waves (Greenspan, 1956). The wave may also slow and steepen as it moves into shallower waters, with funnelling in bays and tidal estuaries. However, the focus of this paper is to describe and address the meteorological factors relating to the origin of the 28-29 May 2017 meteotsunami, and not to model the ocean wave in detail. We describe the development of the MCS, and its' associated thermodynamic processes, over a period of some 6 hours as it passed over the English Channel, southern England and into the southern North Sea. Furthermore, we briefly discuss how these meteo-events can be modelled and forecast, noting possibilities and difficulties.

Careful analysis of the meteorological observations highlights the physical and thermodynamic processes taking place in association with the driving MCS that caused the meteotsunami. The strong rear-flank downdraft from the MCS, and further evaporative cooling from precipitation, were the most likely causes of the atmospheric low-level gravity wave and rapid surface air-pressure changes. The downdraft cooled the boundary layer air, and raised the elevation of the constant pressure surfaces hydrostatically, with a wave period of about one hour. This is similar to an event described by Marsham et al, (2010). The low-level atmospheric gravity wave then travelled with the storm system,

with its speed and direction at medium levels probably controlled by the storm track in the middle troposphere (700 to 500 hPa for medium level convection), and right of the wind flow by an angle of up to 30 degrees (Aherns, 2007:373; Webb & Pike, 2012). Correlation between the medium-level wind flow and meteotsunami formation has been discussed previously (Tappin et al. 2013; Šepić et al. 2015; Sibley et al. 2016). This paper further describes the physics of how energy at medium layers is transferred to the ocean surface.

Historical overview

The low-lying coasts around the southern North Sea are susceptible to flooding from storm surges and unusual wave activity. Thousands of deaths were reported in Belgium, the Netherlands and England following the storm surge of 31 January & 1 February 1953 (Quarles and Ufford, 1953). However, storm surges have much longer wave periods and wavelengths than meteotsunamis. The most notable historical meteotsunami, previous to the Dutch 2017 event, was on 5 June 1858 when a tsunami-like wave was reported running from the English Channel to Denmark, with wave runup estimated at 6 m on Danish coasts. The 1858 event had many similar characteristics to that of 2017, in that it occurred in conjunction with a severe thunderstorm and squally winds. Recent research concludes that it was a meteotsunami, and not a geological tsunami such as from an earthquake or a submarine landslide (Newig and Kelletat, 2011; Long, 2015). In recent years, several meteotsunamis have been observed in the North Sea (Sibley, et al. 2016), and English Channel (Tappin, et al. 2013; Williams, et al 2019). The risk of flooding from meteotsunamis, therefore, highlights the need for improved accurate ocean wave modelling for the prediction of these events, especially if sea levels rise as predicted with global warming and the potential for reduced return periods of coastal flooding (Palmer, et al. 2018). Other studies have considered the effect of harbour seicheing in the Dutch Port of Rotterdam following the passage of active cold fronts, and in northerly showery synoptic weather patterns (De Jong et al. 2003; De Jong and Battjes, 2004). There is a genetic relationship between seicheing and meteotsunamis, in that both are forced by atmospheric pressure changes and/or wind stress acting upon the sea surface, but seiching is also dependent upon specific harbour characteristics. Although in their examples the amplitude of harbour waves was greater than 25 cm, the amplitude of the low-frequency ocean waves was of the order of only 10 cm, compared with nearly 90 cm on 28-29 May 2017. The return period of these small low-frequency sea wave events is greater: the authors identified 44 related seiche events in the Port of Rotterdam in the years 1995 to 2001, which is close to seven per year (De Jong et al. 2003; De Jong and Battjes, 2004).

Meteorological situation 29th May 2017

The synoptic pressure and frontal analysis at 0000 UTC on 29 May 2017 (Figure 2) shows an area of high pressure (HA 1021 hPa) over Europe, and a low pressure centre (LB 999 hPa) over the Baltic region. High pressure (HB 1020 hPa) is centred near northern Britain. Associated fronts extend across the Low Countries, and southern Britain, with a developing, small, low pressure centre (LA 1012 hPa) near Brittany, France, and a surface cold front extending southwards towards Spain. Southern England, France and the Low Countries are in a broad warm sector, with an upper cold front and pressure trough over Northern France and the English Channel. This upper cold front had evidently overrun the surface cold front, indicating the presence of a potentially unstable air mass running into the rear of the MCS.

This synoptic pattern is indicative of a ‘Spanish Plume’ event. These events occur periodically over Europe in the spring and summer months, with hot, southerly, winds and thunderstorms moving northwards from Africa and Spain (Lewis and Gray, 2010). Direct surface heating is lost as air moves into the Bay of Biscay and across northern Europe. However, convective cells may continue, and develop into severe MCSs at medium or elevated levels over northern Europe and the British Isles. Typically, cloud bases are above about 2000 m. The release of conditional instability, which helps drive

the elevated MCS, results from medium-level warm advection, with uplift of the plume along isentropic surfaces, together with horizontal convergence. Further enhancement to convection results from cold advection at higher levels, which further destabilises the vertical profile.

Observational reports

Together with images and video clips of the meteotsunami wave, for example at Zandvoort (Figure 1), it was also identified at the Dutch coast from post-processed radar instrumentation, and tide gauges. The wave height, arriving around high tide, was estimated by several sources to be at or over 2 m (Assink et al. 2018; Helzel, 2017; Helzel Messtechnik, 2017; Hydro International, 2017). However, this height is probably an estimation based on the breaking wave and run-up onto the beach. Lower wave heights were recorded at tide gauges along the Dutch coast, and those at Oosterschelde, Scheveningen, and Ijmuiden Buitenhaven (Figure 6a, 6b), recorded an elevation of 0.44 to 0.5 m. With readings averaged over 10 minutes, however, the full height of the wave was not captured (Sluijter et al. 2017). A gauge on the Europlatform (52.0073N/3.4032E), around 60 km from the entrance to the Port of Rotterdam, with one-minute cadence, recorded a wave amplitude of approximately 0.78 m on residuals, and 0.88 m in total water level (Helzel, 2017) (see also note on Table 1).

Elsewhere along the North Sea coast, tide gauges at other locations show evidence of a sea wave running from Calais (29/0050 UTC), on the coast of northeast France, to Hörnum in Germany (29/1015 UTC). There is also evidence of tide gauge anomalies in the English Channel at Jersey (28/2145 UTC), Le Havre and Bologne-Sur-Mer, and in eastern England at Dover, Harwich, and Lowestoft (29/0300 UTC). There is evidence of harbour seicheing for one or two hours on many of the tide gauges. Table 1 gives the time of occurrence and wave amplitude of gauges along the coasts, and locations shown on the map of Figure 3.

The WavE RAdar (WERA), an ocean remote sensing radar system, recorded the meteotsunami at Monster and Ouddorp on the Dutch coast (Helzel, 2017; Helzel Messtechnik, 2017; Hydro International, 2017). The WERA system was developed by Helzel Messtechnik in co-operation with the University of Hamburg to measure tidal currents. The radar sites, managed by the Ministry of Infrastructure and Environment (Rijkswaterstaat) measure tidal flows around the Port of Rotterdam with a frequency of 16.2 MHz. The system was not operationally configured to detect tsunami waves at this location, but reprocessing by Helzel Messtechnik (2017) revealed the meteotsunami signal. If configured in tsunami mode, it is claimed that the system would have given up to 40 minutes warning before the wave arrived on the coast.

On the 28th and 29th May, rain radar images of precipitation show the development of the MCS over northern France and the English Channel, moving east-northeast (Figure 7), and shown on the synoptic analysis by the upper cold front and trough (Figure 2). The developing storm was characterised by heavy rain, with a developing bow-shaped structure most clearly identifiable at 0100 to 0300 UTC with frequent lightning. The most active convective cells are evident on the storm's southern flank, as shown by the brightest, and heaviest precipitation returns, with, soon after midnight, an area of less heavy rain extending across southeast England. In the early hours of the 29th May, the heaviest area of rain narrowed, and became more organised, being associated with a squall line running east-northeast along the English Channel and into the southern North Sea (Figure7). Across the Netherlands, a squall line was evident on the Herwijnen Doppler radar at 29/0441 UTC (not shown) moving with the storm, together with evidence of atmospheric gravity waves (Sluijter et al. 2017). Such a squally gust front is referred to as *derecho*, in Spanish, if sufficiently long-lived (Šepić and Rabinovich, 2014). The association between convective downdrafts and bow-echoes on rain radar was first noted by Fujita (1978; but see also Doswell, 1993, and Klimowski et al. 2004). It is in the period immediately after

midnight on the 29th May that the strongest wind gusts were reported. And it is during this period that bow-shaped echoes became increasingly evident on rain radar images, and indicative of a strong downdraft and gust front. This bow-shaped signal on radar provides an early notification of possible meteotsunami formation.

Evidence from the Trappes (Paris) ascent (Figure 8) and satellite images (Figure 9) shows MCS cloud tops rising into the stratosphere (above 40000ft, 12190 m). However, in a sequence of infra-red images (MSG 10.8 μm) between 29/0200 and 29/0500 UTC a darkening band in the MCS anvil indicates atmospheric descent. Atmospheric descent causes cloud to dissipate, which is indicated by image darkening, in this case running into the rear of the storm system behind the line of heaviest rain radar echoes. These features may indicate the presence of the downdraft at high altitudes, although convective downdrafts are normally modelled from medium levels (~600 hPa) to the surface (Figure 8).

Synoptic observations in the southeast of England show periods of heavy rain, strong, gusty winds and rapidly fluctuating pressure changes taking place over a matter of minutes. As winds temporarily backed anti-clockwise from the northeast at 29/0040 UTC, a gust speed of 35 knots (18 ms^{-1}) from the south-southwest was recorded at Langdon Bay in Kent. The Sandettie Light Vessel in the Dover Strait (51°12'N 1°48'E) reported a wind gust of 72 knots (37 ms^{-1}) in the hour to 29/0200 UTC, although the gust direction is not clear. From personal correspondence, shipping forecasters generally consider the wind observation at this vessel to be reliable, and representative of the locality (Capon, 2003). The synoptic station at Manston in Kent also reported a similar shift in wind direction, with the stronger gusts coinciding with a rapid rise in pressure.

Atmospheric pressure readings from the 29th May, available at per-minute intervals from UK sites, also show the passage of the storm. At Langdon Bay there was a jump of 4.5 hPa in 14 minutes from 0026 to 0040 UTC (with rates of 0.5 to 1 hPa per minute recorded), followed by a fall of 5.4 hPa in the following 35 minutes. Similar pressure changes were recorded at Herstmonceux and Manston, with the largest fall at Manston, where it fell 6.7 hPa from 1018.9 hPa to 1012.2 hPa in 33 minutes (from 0102-0135 UTC) (Figure 4). At these locations, surface temperatures fell by 4–5°C as the pressure rose. From their timing, these changes suggest that a boundary layer, atmospheric gravity wave, was moving towards the east-northeast, with a pressure peak at Hertsmonceux recorded at 28/2357 UTC, and at Langdon Bay at 29/0040 UTC. With the wind backing so strongly to the southwest, it is probable that a rear flank downdraft temporarily penetrated to the surface. Similar pressure changes were reported in high-resolution barometer readings in the Netherlands (Sluijter et al. 2017; Assink et al. 2018).

The speed of movement of the meso-high or low-level gravity wave, as it travelled from Kent to the coast of the Netherlands, can be calculated from the surface observations and rain radar. Between Langdon Bay to Vlissingen, Hoek van Holland and De Kooy, it was in the range 18 to 20 ms^{-1}. The speed correlates reasonably well with steering-level west-southwesterly winds of 35 knots (18 ms^{-1}) at 700 hPa, measured by the Ijmuiden sounding (Figure 10). The gravity wave wavelength was estimated from the pressure readings and the calculated wave speed. At Langdon Bay, for example, where the pressure change covered a period of 45 minutes travelling at 18 ms^{-1}, a wavelength of 49 km may be calculated, and similarly, around 65 km at Manston and Herstmonceux. Superimposed on the longer wavelengths were smaller ones of higher amplitude, around 8 to 23 km, with periods of 7 to 22 minutes, also observable on the Cabauw LIDAR (Figure 11) (Sluijter et al 2017; Assink et al. 2018) and noted in a previous event by Marsham et al. (2010).

An examination of the vertical profile of the atmosphere aids with understanding the processes ongoing with this event MCS. Although the elevated convective cells were moving from the west-southwest

with the steering flow, the near-surface wind (or boundary level wind) ahead of the storm was east-northeast, with a marked directional veer and velocity shear near the top and above the stable boundary layer. This veer may be identified in representative vertical profiles, which are measured by radiosonde balloon ascents, and plotted as tephi-grams. The Ijmuiden (North Netherlands) sounding at 0300 UTC 29 May 2017 (Figure 10) indicates boundary level air with direction from east-northeast and speed 5 to 10 knots, but around the top of the boundary layer there is a marked direction change to the southwest, and an increase in speed to around 35 knots at 700 hPa. The Herstmonceux ascent failed above 700 hPa (Figure 12), possibly due to the lightning and intense precipitation. But it also shows marked directional changes with height, from east-northeast near the surface, to south at 850 hPa, then southwest at 700 hPa. The main cloud base appears to be around 800 hPa, approximately 1900 m, which supports evidence of an elevated MCS, an elevation broadly confirmed by the Cabauw LIDAR data (Figure 11). The strongest gusts at Manston and Langdon Bay also occurred with a marked direction change to the southwest, and then a slower change towards the northeast. Two other atmospheric soundings are available from Beauvecchain, east of Brussels in Belgium (not shown), and Trappes near Paris with validity time 0000 UTC 29 May (Figure 8). The Trappes ascent is considered more representative, but both soundings were ahead of the storm passage, which limits their representation. For example, the Trappes ascent shows evidence of warm advection in mid-layers between 750 and 650 hPa (red shaded area in figure 8), but couldn't identify the cold advection at higher levels at the rear of the storm. An automated calculation of convectively available potential energy (CAPE) from Trappes gives 619 Jkg^{-1}, but Met Office internal chief forecaster's *Model Assessment and Emphasis* suggested 1300 Jkg^{-1} was possible over Kent in the locality of the MCS (Met Office, 2017). Through the conversion of CAPE to kinetic energy an estimate of the speed of updrafts in a MCS can be made (where maximum speed $w_{max} \equiv \sqrt{(2.CAPE)}$.

Modelling the convective processes and atmospheric gravity wave

As noted, the meso-high that developed in this event can be described as a low-level ducted gravity wave, which is induced by a strong rear flank downdraft, and associated with an elevated MCS (Marsham et al, 2010). The paper by Marsham et al, (2010) is quite important in helping to elucidate the physical processes taking place with the event of 28-29 May 2017. Their paper describes a similar convective event that occurred on 24 June 2005, where an elevated convective storm passed over the Chilbolton radar in central southern England and other nearby instrumentation. The authors demonstrated that the associated surface pressure changes were hydrostatically driven, and caused by a rear-inflow jet (RIJ), or slantwise, rear-flank downdraft (Figure 5). However, as far as we know, there was no notable meteotsunami on that occasion because the convective system was observed primarily over land. Lapworth and Osborne, (2017) also describe the passage of a gravity wave over southern England, with a surface pressure rise driven by convective activity. Similar convective systems that have led to meteotsunami formation have occurred in the USA and Europe, and have been described for example by Šepić et al. (2009), Šepić and Rabinovich (2014), and Wertman et al. (2014).

The following discussion will seek to estimate the speed of the convective downdraft, justify the measured pressure rise using the hydrostatic equation, and estimate the speed of the low-level gravity wave. The speed of the rear-flank downdraft with the events of 28-29 May 2017 can be estimated from levels of downdraft CAPE (DCAPE), which can be approximated from manual constructions of the available vertical sounding tephi-grams. Trappes at 29 May 0000 UTC is probably the most representative in this instance (Figure 8). DCAPE is normally estimated from 600 hPa to the surface along the saturated adiabatic lapse rate (SALR) (DCAPE is sometimes referred to negative available potential energy (NAPE) (Doswell, 1993)). In a convective downdraft colder air is brought to lower

levels, and further cooled through evaporative cooling from precipitation, but mixing at lower levels means the descending air is normally unsaturated. A simplified calculation can be expressed as follows:

DCAPE $\equiv -\int_{Zs}^{Zh} g\frac{T-Te}{Te}dz$; and maximum downdraft speed $w_{max} \equiv \sqrt{(2.DCAPE)}$ (Krueger, 2013).

Where g is gravity (9.81 ms^{-1}), Zs is the surface, Zh is the height (4258 m at 611 hPa at Trappes), T is the downdraft temperature assuming a constant SALR (θ_w of 289 K), and Te is the environment temperature. From the Trappes (Paris) ascent (Figure 8), integrating from 4258 m to the surface gives DCAPE of around 914 Jkg^{-1}, and a theoretical maximum gust speed of 42.8 ms^{-1} or 83 knots. Although the maximum gust may be not be realised due to turbulent mixing, the approximation provides support to the gust of 37 ms^{-1} reported at the Sandettie Light Vessel.

The combination of downdraft flow and precipitation, with associated evaporative cooling, increases the low-level atmospheric density and raises the surface air pressure hydrostatically, thereby inducing a gravity wave in the stable undercurrent (Brown, 1979; Knupp, 1985; Marsham et al. 2010). With the event described by Marsham et al. (2010), the induced wave crest ran some 15 km ahead of the downdraft, and on top of the longer wave, shorter ripples of approximately 7 km wavelength were noted. The overall wave structure they described as a *gravity wave without stagnation.* So, in the consideration of Marsham et al. (2010), the observed pressure meso-high may be explained by the hydrostatic effect where the depth of the undercurrent air is increased through downdraft cooling, with further cooling resulting from precipitation and evaporative cooling. Hydrostatic effects are more pronounced in the lowest layers, because of the greater density of air at these levels compared to higher elevations. The observations of the event that Marsham et al. (2010) describe correlate well with those of the MCS system of 28-29 May 2017. The hydrostatic equation can be expressed as:

$dP/dz = -\rho g$, where ρ, the density of dry air = P/RT

dP/dz is the rate of change of pressure with height, g is gravity 9.81 ms^{-1}, T is temperature in K, and R is the specific gas constant for dry air 287 J/kg.K. The rise in pressure is then a matter of determining the difference in density between the downdraft air density ρ and the environment air ρ_e ahead of the MCS, integrated through the depth of the layer, estimated from surface to 1500 m for the gravity wave (~850 hPa).

$\Delta P = \int_{Zs}^{Zh} g(\rho - \rho_e)dz$

As an approximation from the modifications made to the Trappes ascent (Figure 8), the rise in surface pressure of 5 hPa may be explained by an average drop in temperature of 8 K through a depth of around 1500 m (~850 hPa) above the surface, with an average density increase through the layer of approximately 0.03 kgm^{-3}.

In terms of estimating the speed of the low-level gravity wave, the two-level conceptual model described by Marsham et al. (2010) has an atmospheric gravity wave forming in the boundary layer, moving with the medium layer steering winds, and against the low level flow. Marham et al. (2010) also speculate that there may be a degree of self-organising resonance between the MCS generated low-level gravity wave and the storm system steering wind, i.e. the gravity wave moves broadly with the generating storm. The speed of the atmospheric gravity wave (C_{gw}) in the low level flow may be given by the following relationship:

$C_{gw} = \sqrt{(g.\Delta\theta_v.h_o/\theta_v)}$ (Koch *et al*., 1991)

Where g is gravity, θ_v is the virtual potential temperature, h_o is the inversion height. Estimated parameters may be taken from the Trappes and Ijmuiden ascents, so that: $\Delta\theta_v \approx 8$ K, $\theta v \approx 295$ K (for unsaturated air $\theta_v = \theta\ (1+0.61r)$ where θ is potential temperature, and r is the mixing ratio of water vapour), and estimated boundary layer depth of ho ≈ 900 m +/- 100 m. This gives a wave velocity of 14.6 ms^{-1} at 800 m depth, and 16.4 ms^{-1} at 1000 m depth, with direction towards the east-northeast. However, a correction is appropriate that is dependent upon the amplitude of the wave $(1+ a/2h_o)$ (Baines, 1995: 58). If the gravity wave amplitude is given as a ≈ 500 m, estimated from the Cabauw LIDAR (Sluijter et al. 2017), then this may raise the value by a factor of 1.25 to 1.31, which gives a velocity of 19.2 and 20.5 ms^{-1}. This velocity is not that far from the observed speed of around 18 to 20 ms^{-1}, noting this is with a boundary layer wind component of between 0 and 5 ms^{-1} against the wave direction. Bearing in mind the inherent approximations in this calculation there is at least reasonable agreement with the theory.

Modelling the meteotsunami operationally

Meteotsunamis are generated when a convectively formed atmospheric meso-high causes a depression in the ocean surface, which is then enhanced through Proudman resonance (Proudman, 1929). The enhancement of the meteotsunami is most effective when the speed of the generating storm system *U* matches the speed of the ocean wave, and is usually denoted as the Froude number, where $Fr = U/c \approx 1$ (between 0.9 and 1.1). The speed of the induced ocean wave can be determined through the relation $c= \sqrt{(gh)}$, where g is gravity (9.81 ms^{-1}), and h the depth of water. Williams et al. (2019) for example have modelled a previous event in a study of an event in the English Channel. Post-event modelling has also been undertaken for this 28-29 May 2017 occasion, for instance by Deltares using the Delft 3D suite (Vatvani, 2017; Vatvani, et al. 2018), with simplified wind and air pressure assumptions. From this, a wave was generated moving northeastwards along the coast of eastern England and the Netherlands.

Given the known bathymetry, and a known travelling atmospheric gravity wave, it is potentially feasible to model an induced ocean wave, with enhancement through Proudman resonance, in a coupled ocean-atmosphere high-resolution NWP model, although such a coupled model is not operational at present. However, some uncertainty arises with attempting to model the development of meso-highs in relation to convective systems in deterministic NWP models. The modelling of this MCS within the NWP UKV (approximate 1.5km grid) showed typical divergence in output across two different model runs, with both the operational run and parallel suite (PS39) suggesting the presence of organised showers in southern England. There were clear differences in the location, scale and shape of the forecast convective cells, and a meso-high of 5 hPa was not generated in either (Figure 13). Both the models suggested some small scale variability in pressure near the storm systems, but not the scale of 4 or 5 hPa seen in observations (see Figure 4 and 13).

With a 1.5km grid, which requires a minimum of five grid points to model a gravity wave, there is at least the potential of modelling such features with wavelengths as small as 7 to 15 km. Furthermore, gust fronts were seen in NWP models with convection related to the meteotsunami of 27 June 2011: the UKV at that time forecast a strong downdraft (Tappin et al. 2013). However, there are limits with the ability of high resolution NWP models to accurately model the exact location and size of convection and related phenomena. This is mainly a result of more complex dynamical processes taking place at the scale of convective storms, which requires new mathematical approaches, and still an incomplete understanding of the physics processes within such storm systems. Added to this is a lack of observations at the small scale. Yano et al. (2018) provide a more detailed discussion of the problems and challenges faced. Given such inherent difficulties with deterministic models in predicting the precise location, dynamics and physical processes taking place in convective storms, one way forward

is to utilise ensemble modelling. Multiple model runs in ensembles may at least indicate the possibility of strong downdrafts and low-level gravity waves. At present, however, these models are not available operationally, and an assessment of ensemble modelling has not been carried out.

An alternative approach, considered here, is to use meteorological parameters from the NWP model that have greater certainty to determine the possibility of wave enhancement, where the Froude number $Fr = U/c \approx 1$ (between 0.9 and 1.1). This is described, and illustrated, using a course 2D model with a cross-section of water depth h across the Dover Strait between Dover and Calais. The bathymetric horizontal resolution used here is at 1.12 km, derived and adapted from a bathymetric cross-section survey used for the Channel Tunnel construction (Rankins and Williams, 2012). The water depth in the Dover Strait varies mainly between 25 and 48 m, with a narrow deeper trench to around 60 to 75 m.

The steering medium-level wind speed U may be applied to a fixed bathymetry to indicate the risk of meteotsunamis where the ocean wave speed $c = \sqrt{(gh)}$. However, this is somewhat uncertain without knowing the full characteristics of the MCS, and may vary between 700 and 500 hPa, thus requiring the judgement of human forecasters at shorter lead times. With this event, from observational rain radar trajectories, the Met Office (2017) chief forecaster's *Model Assessment and Emphasis* (28/2100 UTC) suggested 600 hPa was a good representative height for the MCS steering wind flow. A third controlling parameter, such as a large value of CAPE, is necessary to identify only those occasions when a meteotsunami is possible. A risk factor may then be determined through post-processing of the NWP output where CAPE values are high, and where $Fr=U/c \approx 1$ (between 0.9 and 1.1). To assess the validity of this, a simple 2D model is shown in (Figure 14). With this event, a sufficiently large value of CAPE was present >600 Jkg^{-1}, and the steering wind speed estimated to be around 18 to 20 ms^{-1} from rain radar trajectories.

Given an estimated storm movement of 18 ms^{-1} with the medium level steering winds, then Proudman resonance is most effective at a water depth of 33 m (-5 m / +7 m); and 41 m (-7 m / +9 m) depth at 20 ms^{-1}, which correlates well with the actual bathymetry. At 18 ms^{-1}, two areas appear where Fr approaches 1.0 on both sides of the Channel, with the larger area on the English side, while at 20 ms^{-1} the larger area is on the French side, and moving towards the centre of the Dover Strait. At higher speeds of 22 to 26 ms^{-1} this central location becomes more pronounced, but then the Froude correlation is lost above 26 ms^{-1}. Overall, in the Dover Strait Proudman resonance is restricted to occur at wind speeds mainly between 16 and 26 ms^{-1}.

Forecasting capability may also be improved through use of observations and nowcasting tools, such as rain radar, ocean wave radar, and surface observations of pressure and wind at high cadence. Developing storms systems and associated pressure waves may be observed by forecasters in real time, with the possibility of recognition of bow-shaped rain echoes, gusty winds and sudden rises in pressure near convective storms. This gives the possibility of issuing warnings with higher confidence, but with a shorter lead time. Two of the authors here commented on the possibility of the formation of a meteotsunami just prior to this event when the travelling pressure anomaly was observed running along the English Channel. But with no formal notification process in place further action was not possible.

Summary

This 2017 'Dutch' meteotsunami provides an excellent opportunity to understand the generation of a meteotsunami in northwest Europe in detail, where there is high-resolution meteorological data, and video recording of the wave striking the coast. This meteotsunami developed in association with elevated convective storm conditions as part of a 'Spanish Plume': the MCS storm originating over

Spain and the Bay of Biscay, then running along the English Channel and into the southern North Sea. The observational evidence suggests the presence of an atmospheric low-level gravity wave or meso-high running with the elevated MCS. This meso-high, identified by a bow-shaped echoes on rain radar, evidently formed from the hydrostatic effect resulting from the occurrence of a rear flank downdraft and evaporative cooling. As a result of the convective downdraft, and surface pressure rise, energy was transferred from medium levels into the ocean through the reverse pressure effect. The wave was then enhanced through Proudman resonance.

With increasing evidence of the meteorological factors generating such low-level gravity waves, it is desirable to model such events in high-resolution NWP models. But with these models there are inherent challenges because of limitations in the deterministic models ability to forecast the exact shape and location of convective storms systems. However, because of resonant interaction with the water surface, which is dependent upon the forecast speed of the storm, the co-located low-level gravity wave, and the known water depth, there is potential for modelling and forecasting the risk of meteotsunamis through post-processing from NWP output. This will give sufficient notice to issue alerts and warnings. To illustrate this a simple 2D model is described here based on values of CAPE, medium level winds and a fixed bathymetry. There is also the potential of using nowcasting tools, such as rain radar together with observations of surface wind and pressure, to identify events in real time, so that alerts with greater confidence, but shorter lead times may be issued.

Acknowledgements

Thanks to colleagues Martin Young, Matt Lehnert and Nigel Bolton for advice and comments, and to Jelle Assink and Rob Sluijter for information and provision of the LIDAR image. Tide gauge graphs were provided by Rijkswaterstaat, and the Cabauw Lidar and Ijmuiden radiosonde tephigram by KNMI - CC0 statement. Other tide gauge data has been sourced from the EU JRC. Tephigrams were sourced through the University of Wyoming. Rain radar, satellite imagery, and NWP model data is courtesy of Met Office. The photo of the meteotsunami wave is from Jan Koning. The Bathymetry map is sourced via the NOAA NCEI. DRT publishes with permission of the CEO of the British Geological Survey (United Kingdom Research and Innovation). © Crown copyright.

Declaration of Conflict of Interest

Andrew Sibley and Dave Cox carried out this research while in the regular employment of the Met Office; David Tappin within the regular employment of the British Geological Survey. Andrew Sibley is on the editorial board of the Royal Met. Soc. *Weather* journal. The authors have no conflicts of interest to declare that are relevant to the content of this article.

References

Aherns CD (2007) Meteorology Today: An Introduction to Weather, Climate and the Environment, 8th edition, Thomson Learning Inc., Belmont CA

Assink J, Evers L, Smink M, Apituley A (2018) High-Resolution Observations of a Meteo-Tsunami, Geophysical Research Abstracts, 20:11848, EGU 2018 General Assembly

Brown JM (1979) Mesoscale unsaturated downdrafts driven by rainfall evaporation: A numerical study, J. Atmos. Sci., 36:313-338

Churchill DD, Houston SH, Bond NA (1995) The Daytona Beach wave of 3- 4 July 1992: a shallow- water gravity wave forced by a propagating squall line. Bull. Am. Met. Soc. 76:21– 32

441 Capon, RA (2003) Wind speed-up in the Dover Straits with the Met Office New Dynamics Model,
442 Meteorol. Appl. 10:229–237

443 De Jong MPC, Holthuijsen LH, Battjes JA (2003) Generation of seiches by cold fronts over the
444 southern North Sea, J Geophys Res, 108: C43117. http://doi:10.1029/2002JC001422

445 De Jong MPC, Battjes JA (2004) Low-frequency sea waves generated by atmospheric convection
446 cells, J Geophys Res, 109: C01011. http://doi:10.1029/2003JC001931

447 Doswell CA, (1993) Extreme Convective Windstorms: Current Understanding and Research,
448 Proceedings, Spain-U.S. Joint Workshop on Natural Hazards, Barcelona, Spain, 8-11 June 1993

449 Fujita, TT (1978) Manual of downburst identification for Project NIMROD, SMRP research paper
450 156, University of Chicago, Chicago, 1 May 1978.

451 Greenspan HP (1956) The generation of edge waves by moving pressure distributions. J. Fluid Mech.
452 1:574–592. http://doi:10.1017/S002211205600038X.

453 Helzel T (2017) Tsunami detection: Meteo Tsunami, Met Tech Int, September, 161–162.

454 Helzel Messtechnik (2017) 'Mini Tsunami' detected by ocean radar WERA – 40 minutes before it
455 flooded Dutch beeches, *Press Release*, Kaltenkirchen, Germany, July. https://helzel-
456 messtechnik.de/files/432/upload/Pressreleases/2017/Helzel-MeteoTsu-MetTech-2017-FINAL.pdf .
457 Accessed 23 April 2020.

458 Houze RA, Rutledge SA, Biggerstaff MI, Smull BF (1989) Interpretation of Doppler weather radar
459 displays of midlatitude mesoscale convective systems. Bull Amer Meteor Soc, 70:608–619

460 Hydro International (2017) Mini Tsunami Detected Using Wave Radar, Hydro International, Geomares,
461 Lemmer, Netherlands, 17 July. https://www.hydro-international.com/content/news/mini-tsunami-
462 detected-using-wave-radar. Accessed 10 November 2019

463 Klimowski BA, Hjelmfelt MR, Bunkers MJ (2004) Radar Observations of the Early Evolution of
464 Bow Echoes, Weather and Forecasting, 19:727–234

465 Knupp KR, Cotton WR (1985) Convective Cloud Downdraft Structure: An Interpretive Survey, Rev
466 Geophys, 23:183–215

467 Koch SE, Dorian PB, Ferrare R, Melfi SH, Skillman WC, Whiteman D (1991) Structure of an internal
468 bore and dissipating gravity current as revealed by Raman lidar, Monthly Weather Review, 119:857–
469 887

470 Krueger SK (2013) Convective Outflows–Atmospheric Sciences 6150, Dept of Atmos Sciences,
471 University of Utah, Salt Lake City

472 Lapworth A, Osborne SR (2017) An atmospheric bore passing over southern England?, Weather,
473 72:310–314.

474 Lewis MW, Gray SL (2010) Categorisation of synoptic environments associated with mesoscale
475 convective systems over the UK, Atmos Res, 97(1-2):194–213

476 Markowski P, Richardson Y (2011) Mesoscale Meteorology in Midlatitudes, Wiley-Blackwell,
477 Oxford

Marsham JH, Browning KA, Nicol JC, Parker DJ, Norton EG, Blyth AM, Corsmeier U, Perry FM (2010) Multi-sensor observations of a wave beneath an impacting rear-inflow jet in an elevated mesoscale convective system. QJR Meteorol Soc, 136: 1788–1812. http://doi:10.1002/qj.669

Met Office (2017) Model Assessment and Emphasis, 28 May 2019, 2100 UTC, Exeter.

Monserrat S, Vilibić I, Rabinovich AB (2006) Meteotsunamis: Atmospherically induced destructive ocean waves in the tsunami frequency band. Natural Hazards and Earth System Sciences, 6:1035-1051

Palmer M, Howard T, Tinker J, Lowe J, Bricheno L, Calvert D, Edwards T, Gregory J, Harris G, Krijnen J, Pickering M, Roberts C, Wolf J (2018) UKCP18 Marine report, November 2018. EA and Met Office, Exeter

Pattiaratchi CB, Wijeratne EMS (2015) Are meteotsunamis an underrated hazard? Phil Trans Royal Soc A, 373:20140377, 28 October 2015, https://doi.org/10.1098/rsta.2014.0377

Proudman J (1929) The effects on the sea of changes in atmospheric pressure. Geophys Suppl Mon Notices R, Astr Soc, 2:197– 209.

Quarles HA, Ufford V (1953) The Disastrous Storm Surge of 1 February, Weather, 8:116–120

Rabinovich AB (2020) Twenty-seven years of progress in the science of meteorological tsunamis following the 1992 Daytona Beach event, Pure and Appl Geophys, 177(3):1193-1230; http://doi.org/10.1007/s00024-019-02349-3.

Rankins B, Williams R (2012) Channel Tunnel, The Geological Society, Mott MacDonald. https://www.geolsoc.org.uk/GeositesChannelTunnel Accessed April 2020.

Šepić J, Vilibić I, Belušić D (2009) Source of the 2007 Ist meteotsunami (Adriatic Sea), J Geophys Res, 114, C03016, http://doi:10.1029/2008JC00509

Šepić J, Rabinovich AB (2014) Meteotsunami in the Great Lakes and on the Atlantic coast of the United States generated by the “derecho” of June 29–30, 2012, Natural Hazards, 74:75–10.

Šepić J, Vilibić I, Rabinovich AB, Monserrat S (2015) Widespread tsunami-like waves of 23-27 June in the Mediterranean and Black Seas generated by high-altitude atmospheric forcing, Scientific Reports, 29 June 2015, 5:11682, http://doi:10.1038/srep11682

Sibley A, Cox D, Long D, Tappin D, Horsburgh K (2016) Meteorologically generated tsunami-like waves in the North Sea on 1/2 July 2015 and 28 May 2008, Weather, 71, 68–74. http://doi:10.1002/wea.2696.

Sluijter R, Schrier G, Assink J, Veen B, Evers L, Apituley A, Thijm S (2017) Meteo-tsunami hits the Dutch coast, June 7, https://www.knmi.nl/kennis-en-datacentrum/achtergrond/meteo-tsunami-treft-nederlandse-kust. Accessed 23 April 2020.

Tappin DR, Sibley AM, Horsburgh K, Daubord C, Cox D, Long D (2013) The English Channel 'tsunami' of 27 June 2011 - a probable meteorological source, Weather, 68: 144–152, http://doi:10.1002/wea.206

514 Vatvani D (2017) Simulation meteo-tsunami 29 May 2017 along Dutch coast, 5 July,
515 https://www.deltares.nl/en/news/simulation-meteo-tsunami-29-may-2017-along-dutch-coast/.
516 Accessed 10 November 2019).

517 Vatvani D, Dongeren AV, Kroos Sr J, Ormondt, MV (2018) Simulation of 2017 meteo-tsunami event
518 along the Dutch Coast, 2018 Ocean Sciences Meeting, Portland, Oregon, 11-16 February.

519 Webb JDC, Pike WS (2012) Thunderstorms and hail on 7 June 1996: An early season 'Spanish
520 plume' event, Weather, 53:234–241.

521 Wertman CA, Yablonsky RM, Shen Y, Merrill J, Kincaid CR, Pockalny R (2014) Mesoscale
522 convective system surface pressure anomalies responsible for meteotsunamis along the U.S. East
523 Coast on June 13th, *Scientific Reports*, 4:7143. http://doi:10.1038/srep07143.

524 Williams DA, Horsburgh KJ, Schultz DM, Hughes CW (2019) Examination of Generation
525 Mechanisms for an English Channel Meteotsunami: Combining Observations and Modeling, J. Phys.
526 Oceanography, 49:103–120, http://doi:10.1175/JPO-D-18-0161.1

527 Yano J, Ziemiański MZ, Cullen M, Termonia P, Onvlee J, Bengtsson L, Carrassi A, Davy R, Deluca
528 A, Gray SL, Homar V, Köhler M, Krichak S, Michaelides S, Phillips VT, Soares PM, Wyszogrodzki
529 AA, 2018: Scientific Challenges of Convective-Scale Numerical Weather Prediction. *Bull. Amer.*
530 *Meteor.* Soc., 99: 699–710, https://doi.org/10.1175/BAMS-D-17-0125.1

531

Table 1. Location	Date & time of initial wave peak (UTC)	Maximum Amplitude from tide residuals	Report cadence
Jersey, Channel Islands	28-5-17 2145	0.18 m	15 min
Le Havre 2, France	28-5-17 2251	0.26 m	1 min
Boulogne-Sur-Mer 2, France	29-5-17 0022	0.53 m	1 min
Calais, France	29-5-17 0050	0.72 m	1 min
Dunkerque, France	29-5-17 0125	0.4 m	1 min
Ostende, Belgium	29-5-17 0215	0.44 m	5 min
Oosterschelde, NL	29-5-17 0210	0.46 m (est.)	10 min
Scheveningen, NL	29-5-17 0300	0.5 m (est.)	10 min
Ijmuiden, NL	29-5-17 0330	0.44 m (est.)	10 min
Europlatform, NL	29-5-17 0245	0.78 m / 0.88 m (est.) *	1 min
Helgoland, Germany	29-5-17 0910	0.33 m	1 min
Hörnum, Germany	29-5-17 1015	0.24 m	1 min
Dover, England	29-5-17 0030	0.11 m	15 min
Harwich, England	29-5-17 0230	0.12 m	15 min
Lowestoft, England	29-5-17 0300	0.25 m	15 min
(est.) = estimated: the wave amplitude for the Netherland tide gauges (managed by Rijkswaterstaat) has been extrapolated from the graphs of Sluijter et al. (2017), and Helzel (2017). The Europlatform graph shows the total water change, and residual change. Other data has been sourced via the EU JRC. * The residual one minute data at Europlatform seems to have been subtracted from the ten minute mean, which is also subject to the meteotsunami wave activity, therefore the estimated 0.78 m residual is possibly not the true residual, and 0.88 m may be closer to the actual residual.			

Table 1. Tide gauge data from gauges in France, Channel Islands, England, Belgium, Netherlands and Germany. Times are in UTC, amplitude of the wave is metres, and report period in minutes. The wave can be traced over a period of over 12 hours from Jersey to Hörnum, with peak amplitudes reported at Calais and Europlatform.

Figure 1

Click here to access/download;Figure;Figure 1. .bmp

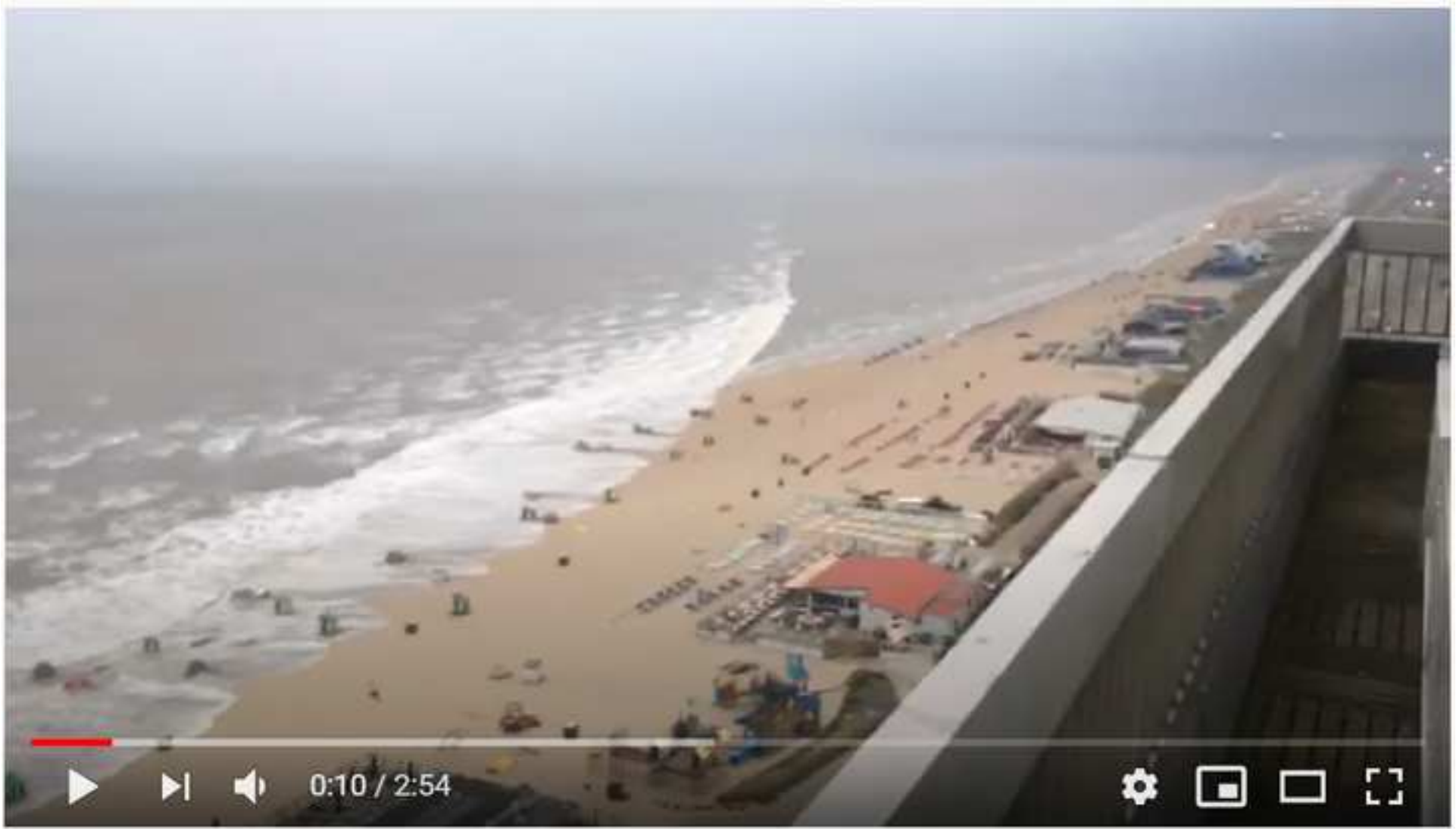

Figure 2

Click here to access/download;Figure;Figure 2..bmp

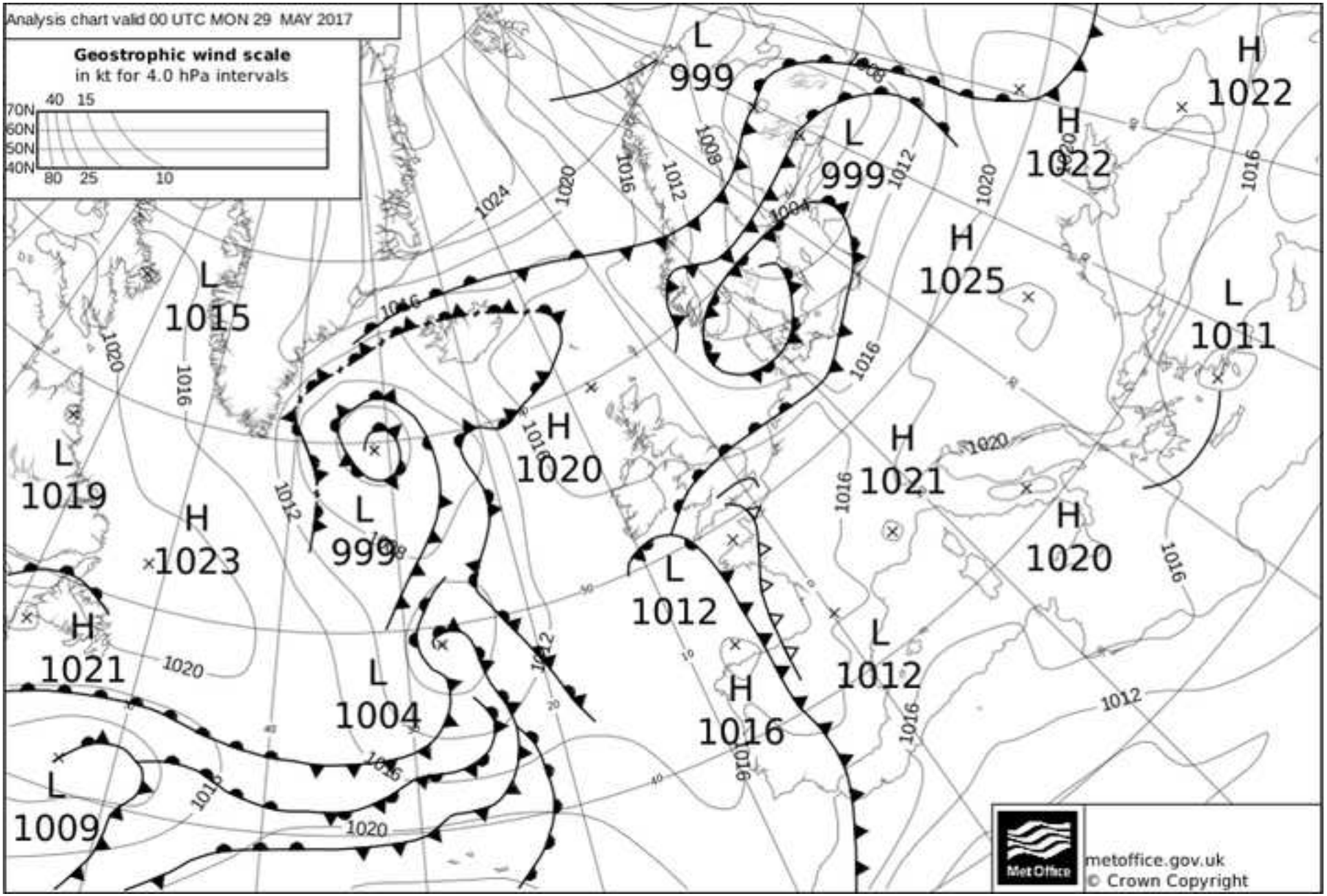

Figure 3

Click here to access/download;Figure;Figure 3..png

Figure 4

Click here to access/download;Figure;Figure 4..png

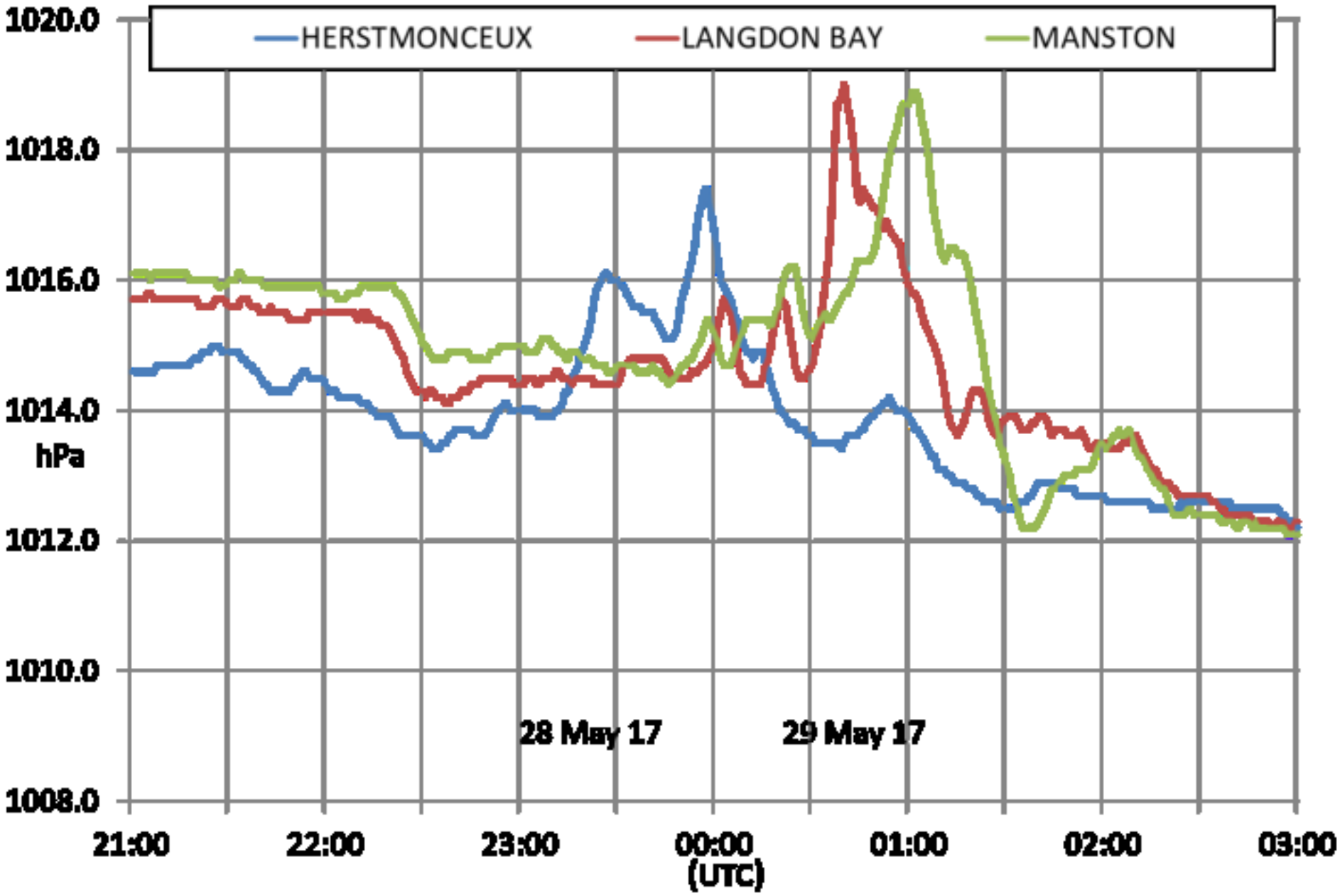

Figure 5

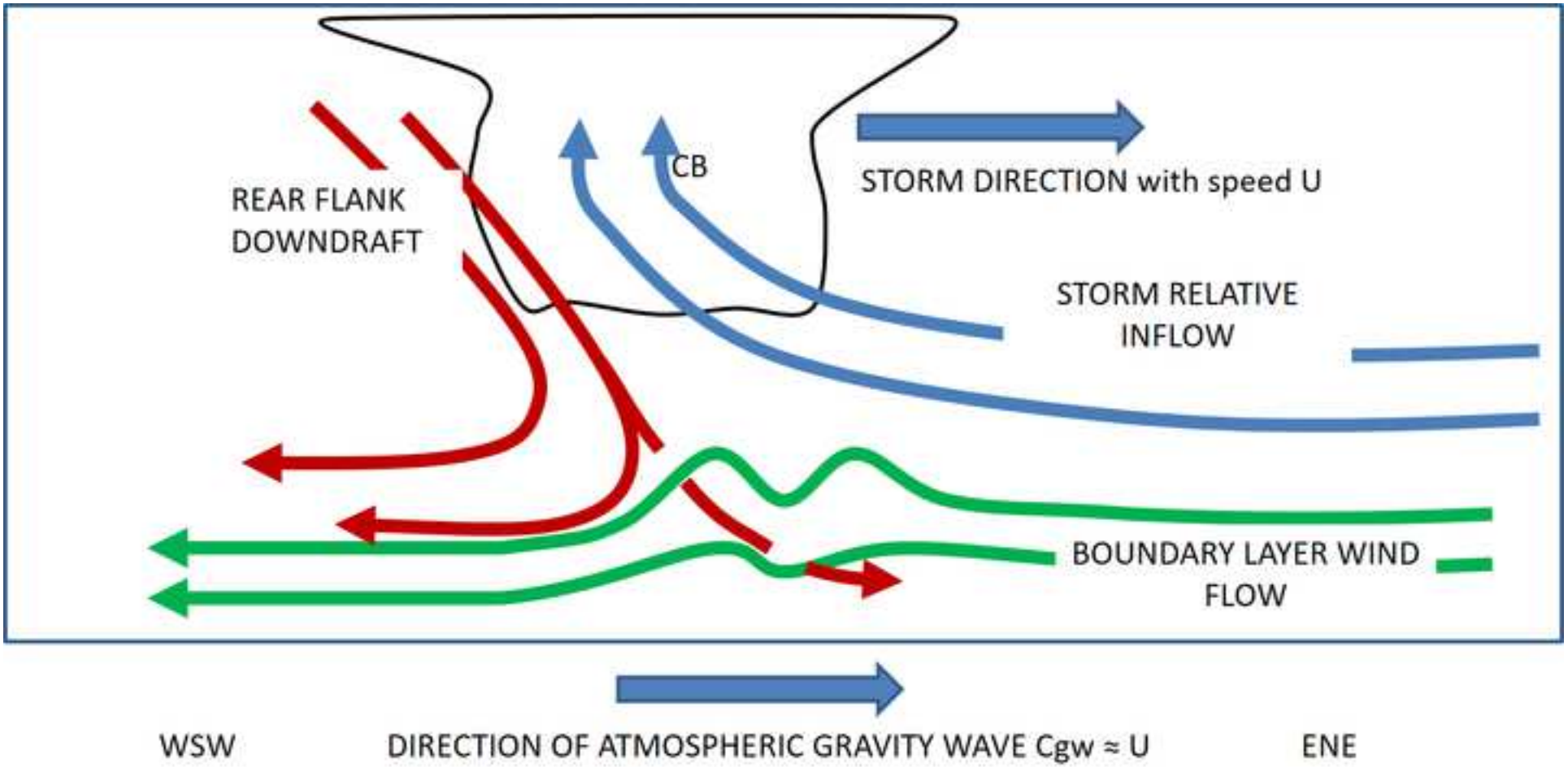

Figure 6a

Click here to access/download;Figure;Figure 6a..bmp

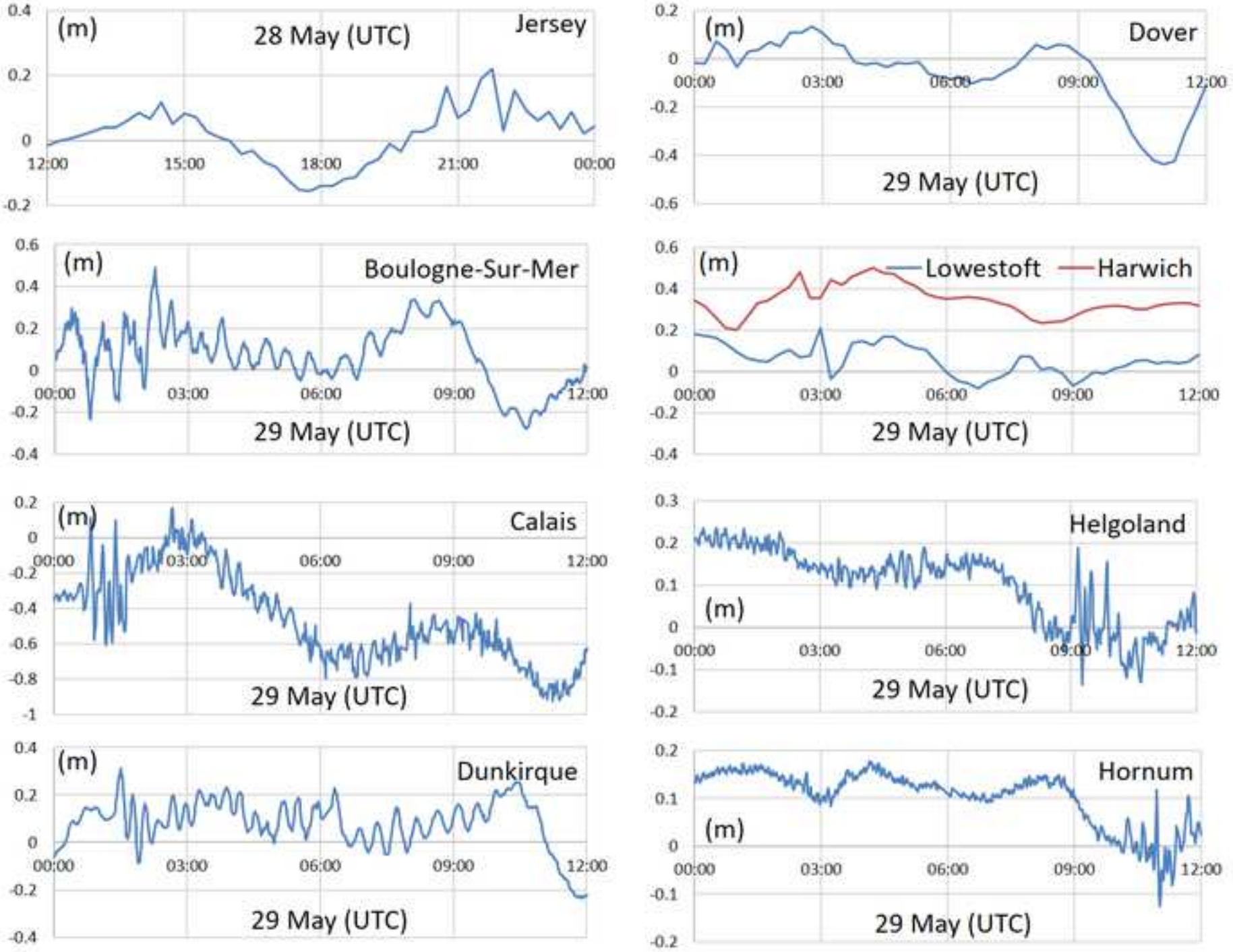

Figure 6b

Click here to access/download;Figure;Figure 6b.bmp

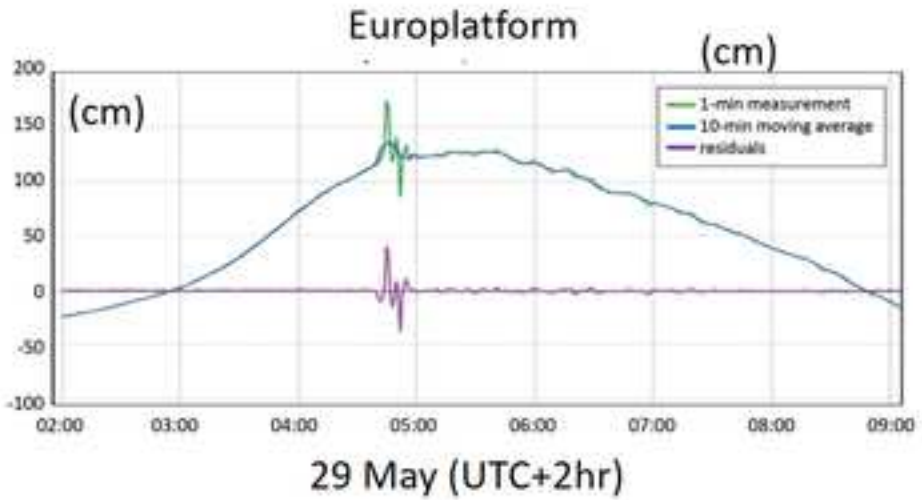

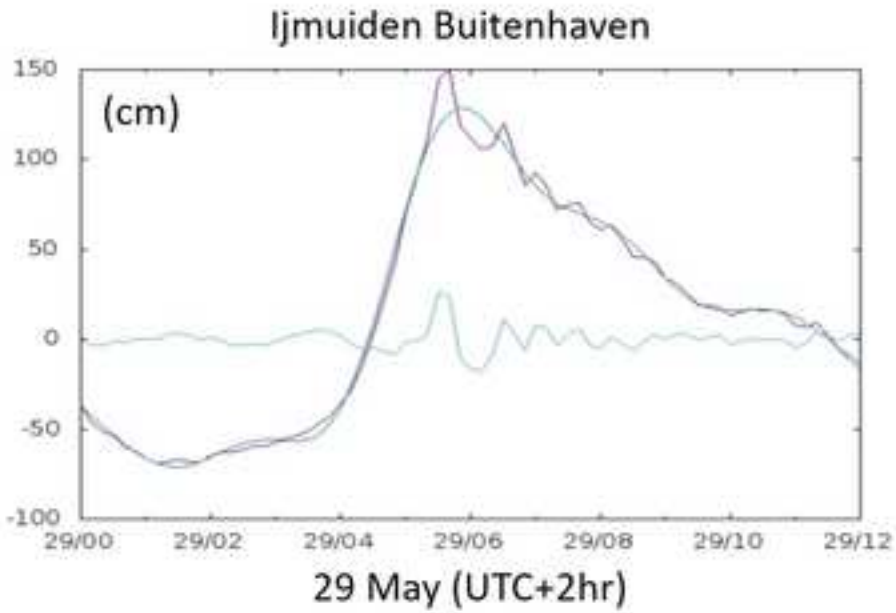

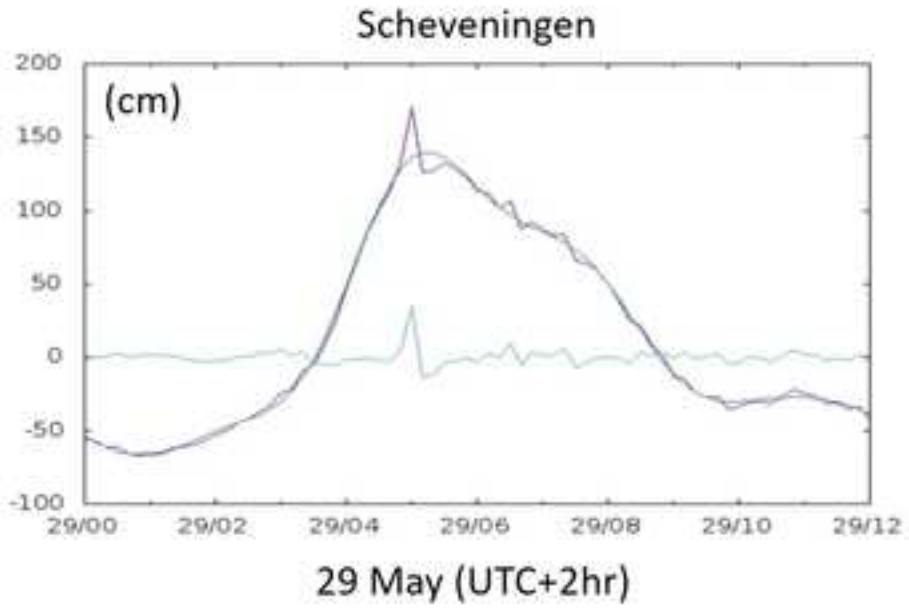

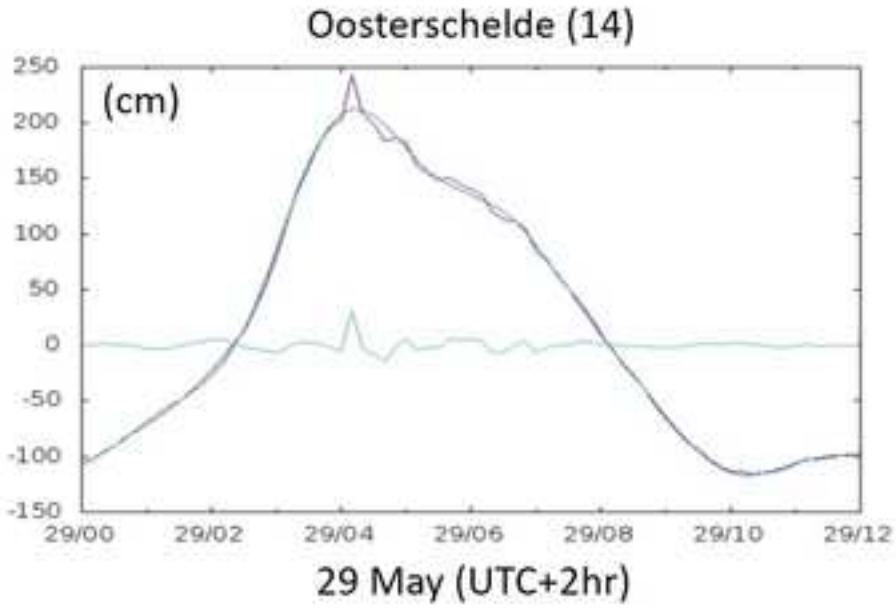

Figure 7

Click here to access/download;Figure;Figure 7..png

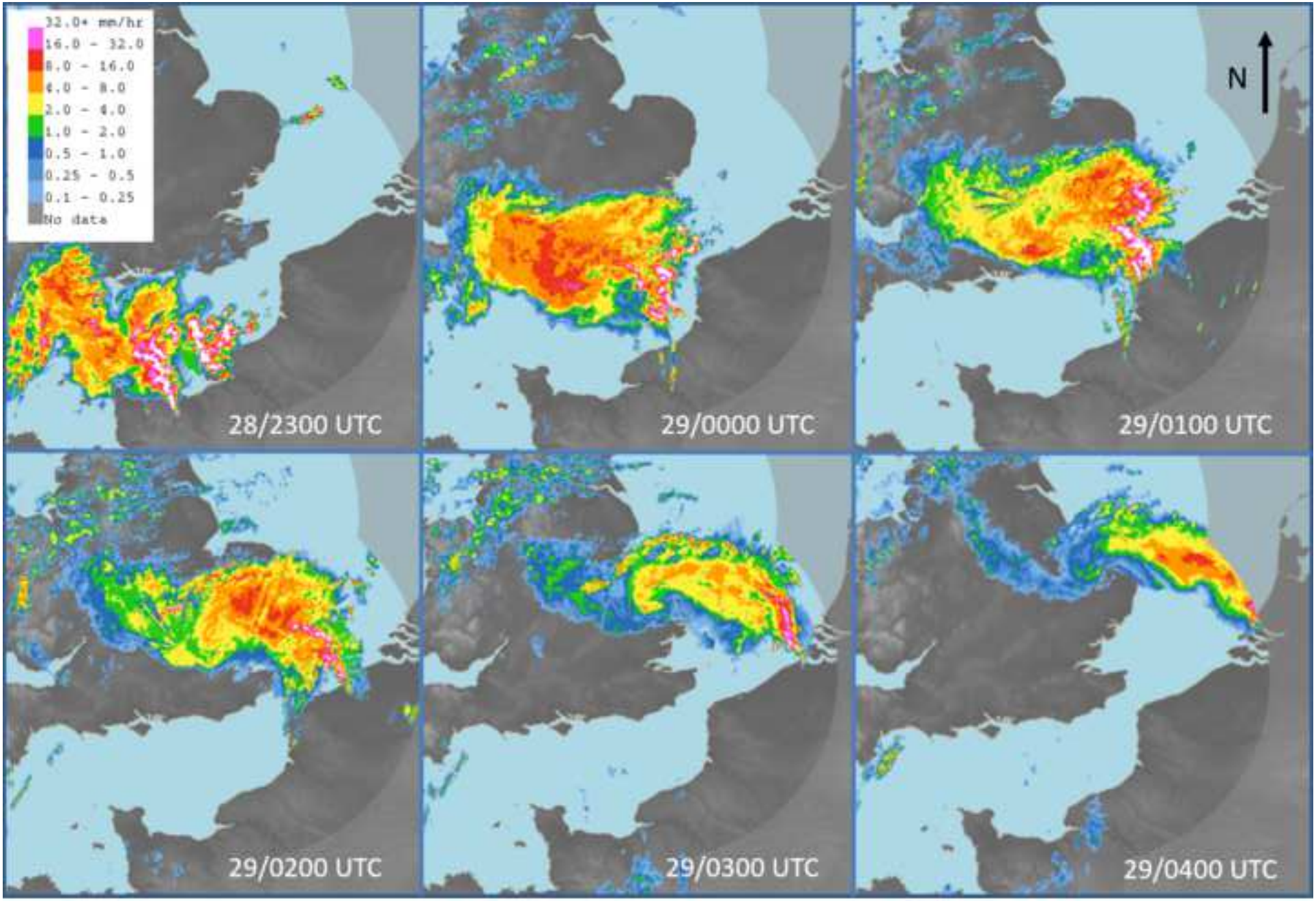

Figure 8

Click here to access/download;Figure;Figure 8..bmp

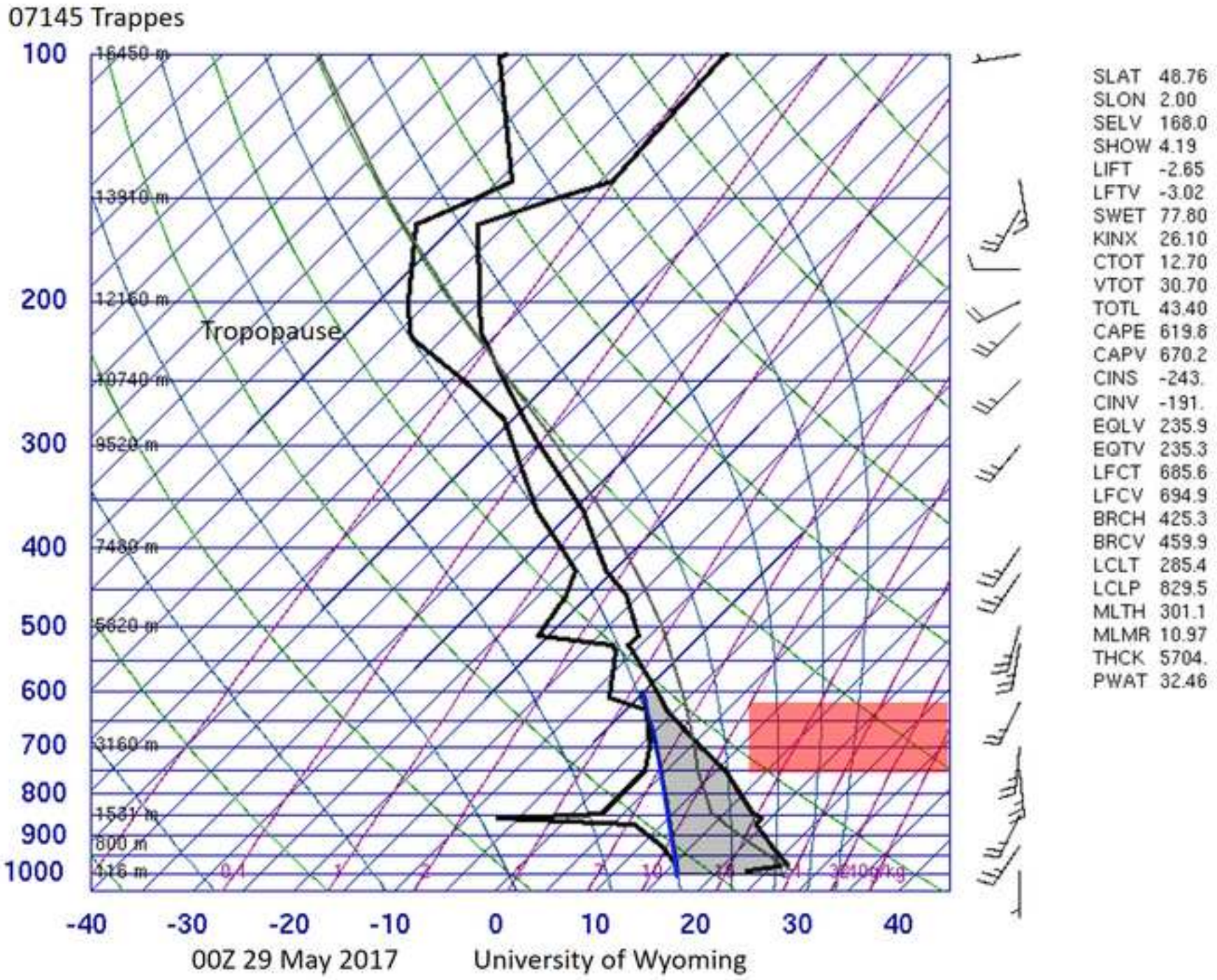

Figure 9

Click here to access/download;Figure;Figure 9..bmp

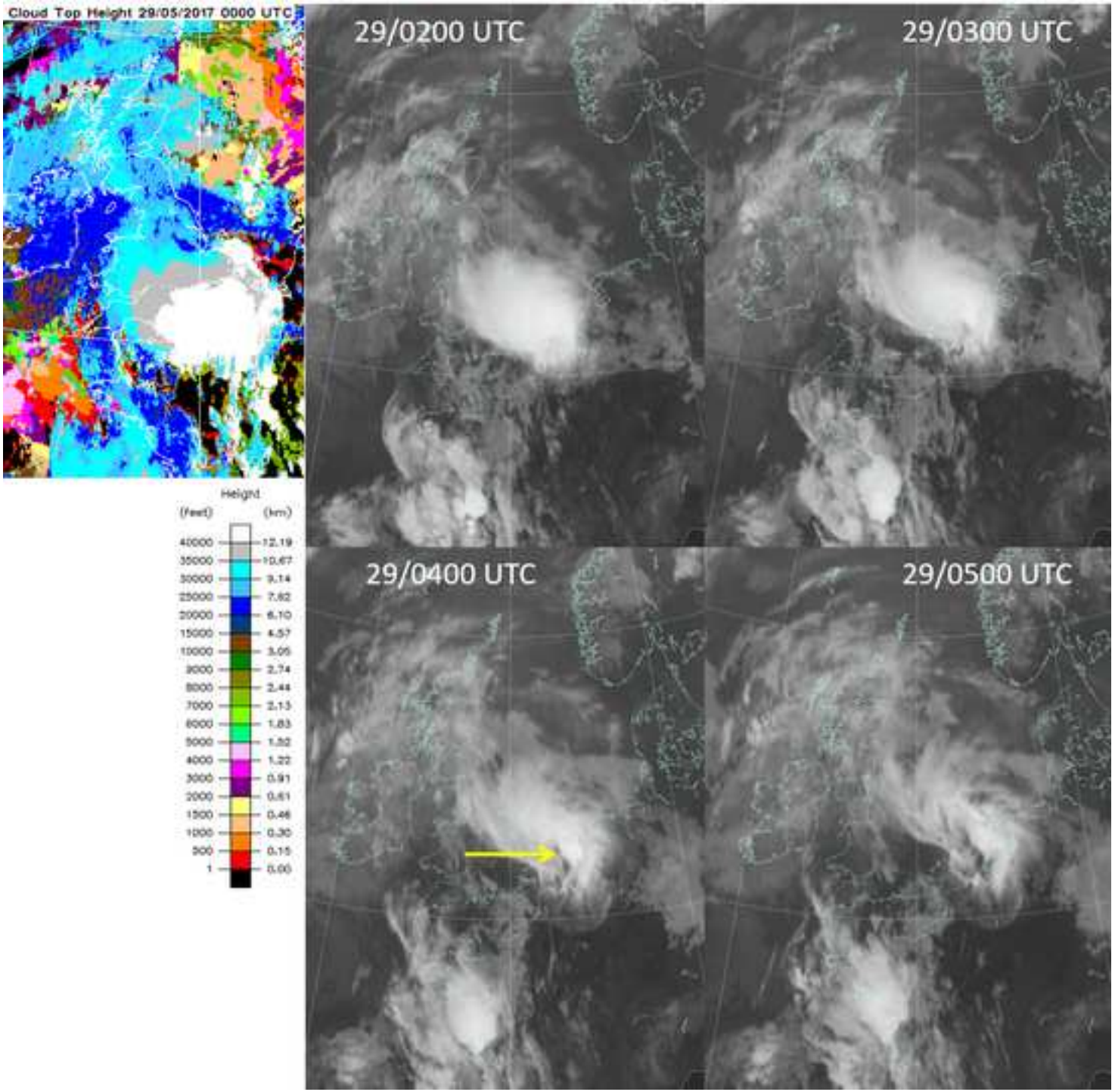

Figure 10

Click here to access/download;Figure;Figure 10.bmp

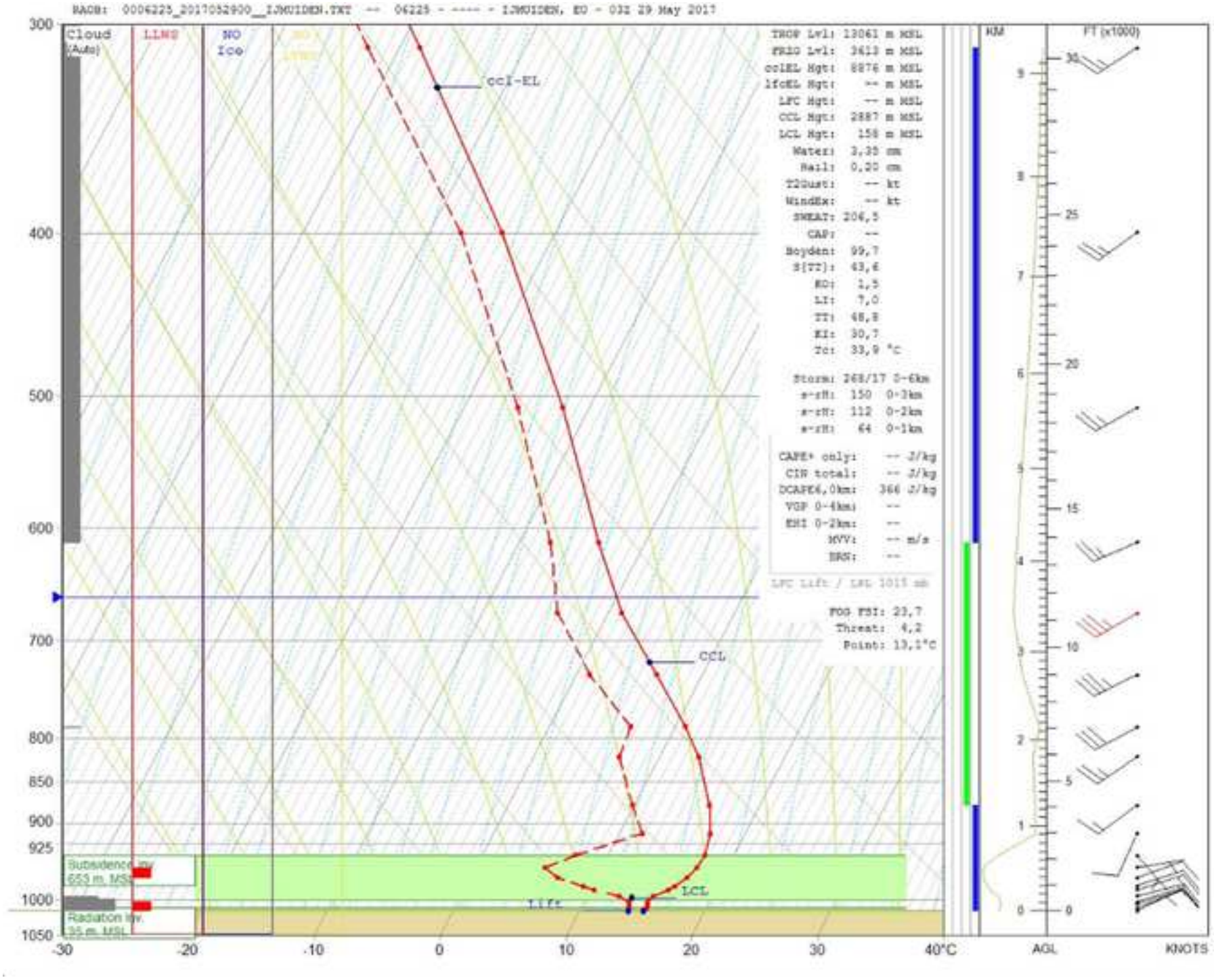

Figure 11

Click here to access/download;Figure;Figure 11..bmp

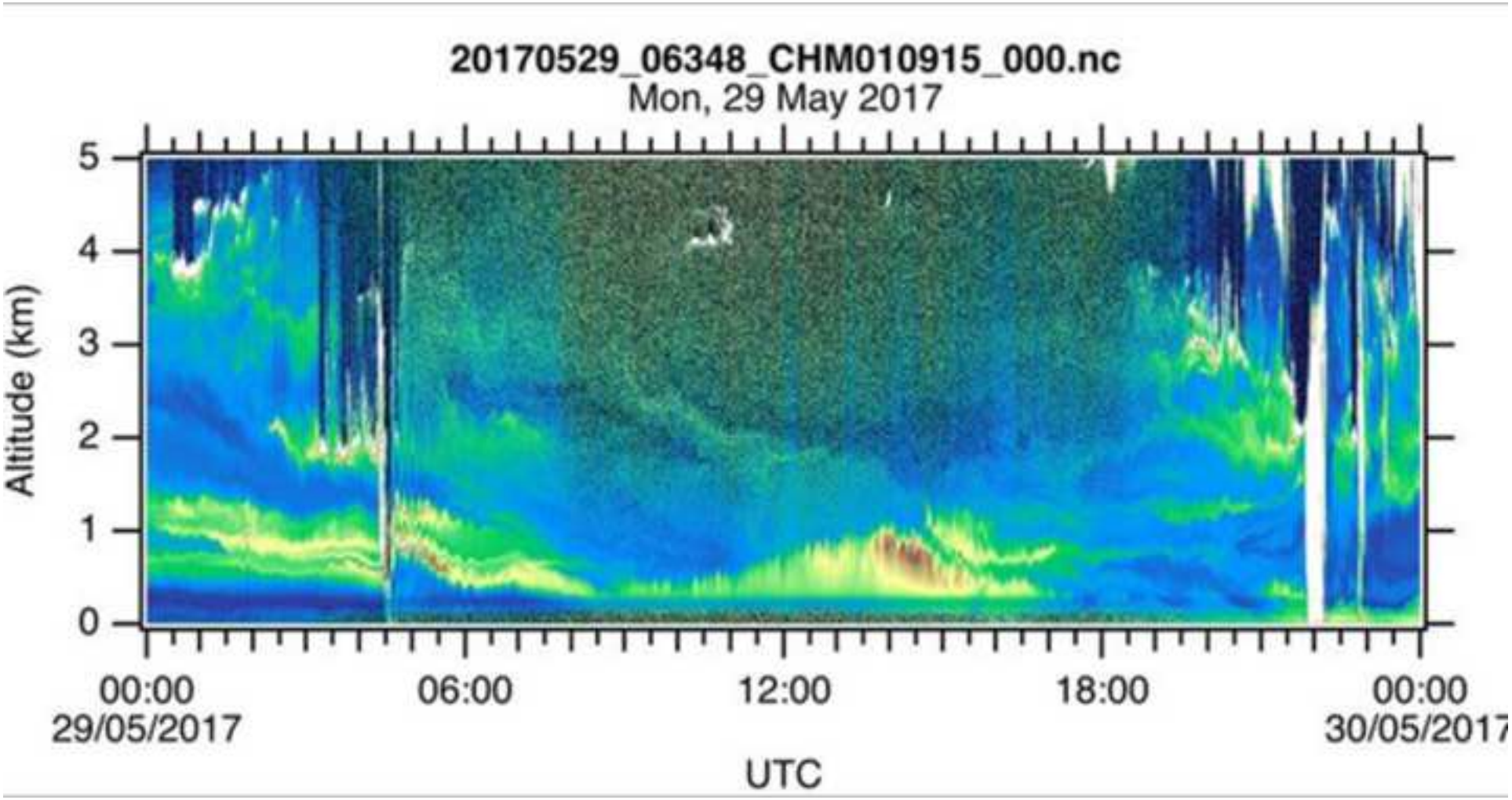

Figure 12

Click here to access/download;Figure;Figure 12..bmp

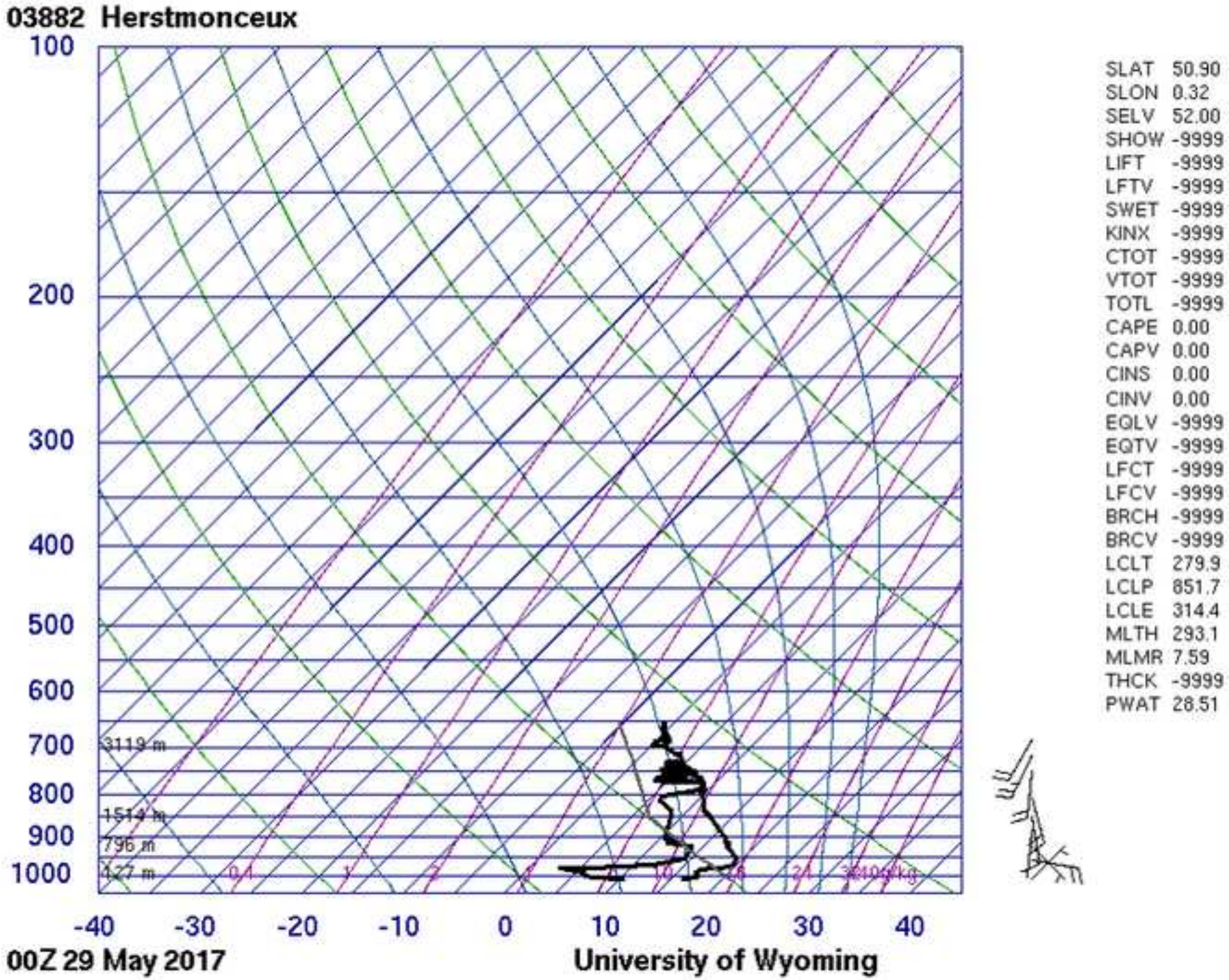

Figure 13

Click here to access/download;Figure;Figure 13.bmp

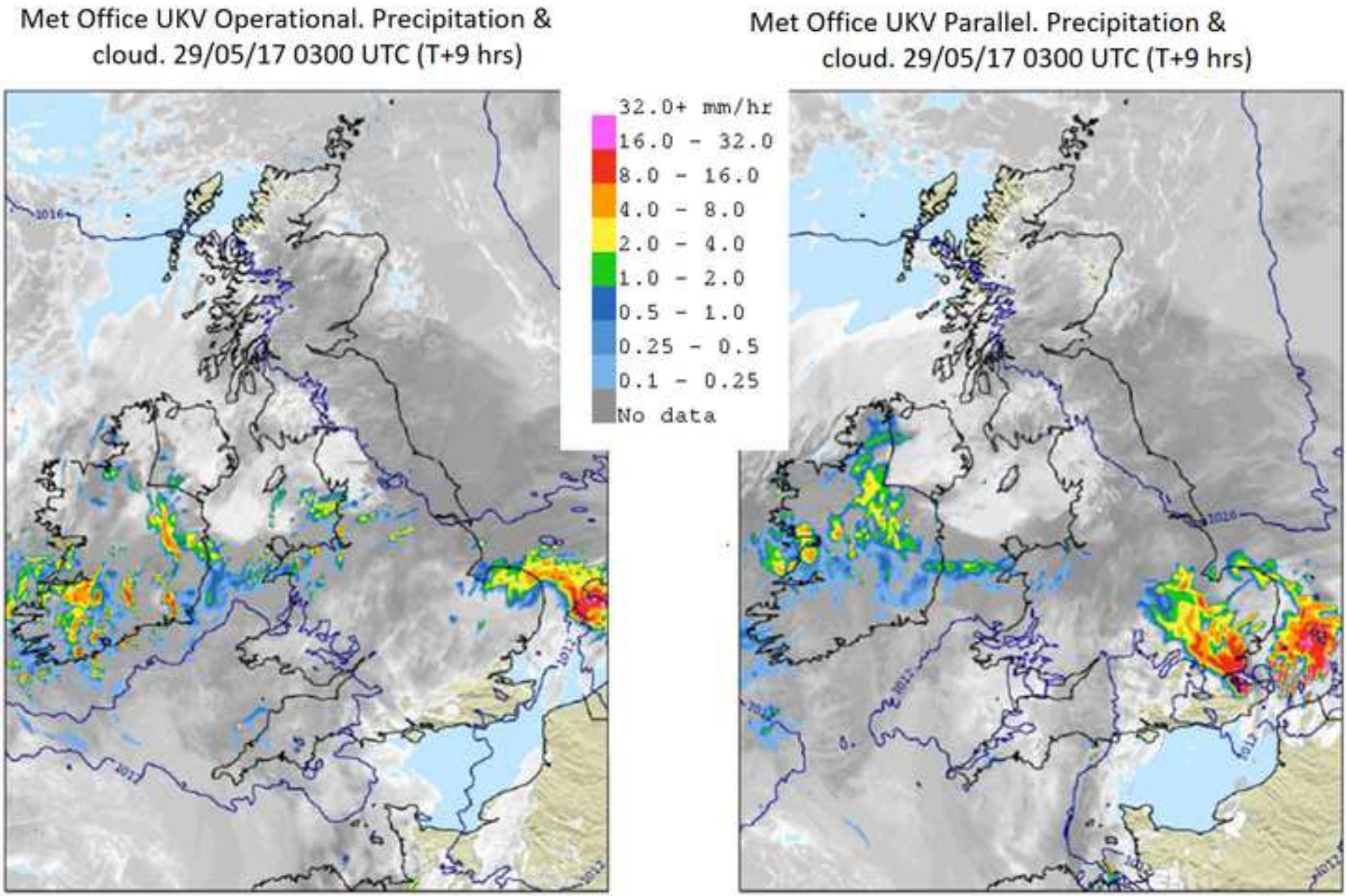

Figure 14

Water depth (m)	19	24	29	29	29	29	29	33	38	33	38	48	52	57	57	57	57	62	57	48	48	48	48	43	43	48	38	33	29	29	24	19	10
Wave speed (ms-1)	14	15	17	17	17	17	17	18	19	18	19	22	23	24	24	24	24	25	24	22	22	22	22	21	21	22	19	18	17	17	15	14	10
U/c at 14 ms-1	1.02	0.92	0.84	0.84	0.84	0.84	0.84	0.77	0.72	0.77	0.72	0.65	0.62	0.59	0.59	0.59	0.59	0.57	0.59	0.65	0.65	0.65	0.65	0.68	0.68	0.65	0.72	0.77	0.84	0.84	0.92	1.02	1.45
U/c at 16 ms-1	1.17	1.05	0.96	0.96	0.96	0.96	0.96	0.88	0.83	0.88	0.83	0.74	0.71	0.68	0.68	0.68	0.68	0.65	0.68	0.74	0.74	0.74	0.74	0.78	0.78	0.74	0.83	0.88	0.96	0.96	1.05	1.17	1.66
U/c at 18 ms-1	1.32	1.18	1.08	1.08	1.08	1.08	1.08	1.00	0.93	1.00	0.93	0.83	0.79	0.76	0.76	0.76	0.76	0.73	0.76	0.83	0.83	0.83	0.83	0.88	0.88	0.83	0.93	1.00	1.08	1.08	1.18	1.32	1.86
U/c at 20 ms-1	1.46	1.31	1.19	1.19	1.19	1.19	1.19	1.11	1.03	1.11	1.03	0.93	0.88	0.84	0.84	0.84	0.84	0.81	0.84	0.93	0.93	0.93	0.93	0.98	0.98	0.93	1.03	1.11	1.19	1.19	1.31	1.46	2.07
U/c at 22 ms-1	1.61	1.44	1.31	1.31	1.31	1.31	1.31	1.22	1.14	1.22	1.14	1.02	0.97	0.93	0.93	0.93	0.93	0.89	0.93	1.02	1.02	1.02	1.02	1.07	1.07	1.02	1.14	1.22	1.31	1.31	1.44	1.61	2.28
U/c at 24 ms-1	1.76	1.57	1.43	1.43	1.43	1.43	1.43	1.33	1.24	1.33	1.24	1.11	1.06	1.01	1.01	1.01	1.01	0.97	1.01	1.11	1.11	1.11	1.11	1.17	1.17	1.11	1.24	1.33	1.43	1.43	1.57	1.76	2.48
U/c at 26 ms-1	1.90	1.70	1.55	1.55	1.55	1.55	1.55	1.44	1.34	1.44	1.34	1.20	1.15	1.10	1.10	1.10	1.10	1.06	1.10	1.20	1.20	1.20	1.20	1.27	1.27	1.20	1.34	1.44	1.55	1.55	1.70	1.90	2.69
U/c at 28 ms-1	1.98	1.83	1.67	1.67	1.67	1.67	1.67	1.55	1.45	1.55	1.45	1.30	1.24	1.18	1.18	1.18	1.18	1.14	1.18	1.30	1.30	1.30	1.30	1.37	1.37	1.30	1.45	1.55	1.67	1.67	1.83	2.05	2.90
Distance (km)	1.1	2.2	3.4	4.5	5.6	6.7	7.8	9.0	10.1	11.2	12.3	13.4	14.6	15.7	16.8	17.9	19.0	20.2	21.3	22.4	23.5	24.6	25.8	26.9	28.0	29.1	30.2	31.4	32.5	33.6	34.7	35.8	37.0